Proceedings of the ASME 2021
Fluids Engineering Division Summer Meeting
FEDSM2021
August 10-12, 2021, Virtual, Online

FEDSM2021-65177

RANS-VOF SIMULATIONS OF FULLY DEVELOPED DENSITY-STRATIFIED AIR-WATER FLOW IN A 3D RECTANGULAR DUCT

Chandrima Jana Maiti
Dept. of Mechanical & Materials Engineering
University of Cincinnati
Cincinnati, Ohio 45221 USA
janaca@mail.uc.edu

Urmila Ghia
Dept. of Mechanical & Materials Engineering
University of Cincinnati
Cincinnati, Ohio 45221 USA
ghiau@ucmail.uc.edu

Leonid A. Turkevich
National Institute for Occupational Safety and Health
Centers for Disease Control and Prevention
Cincinnati, Ohio 45226 USA
llt0@cdc.gov

Abstract

We perform RANS-VOF simulation of turbulent, fully developed, density-stratified air-water flow in a 3D rectangular duct cross section of height twice the width. Flow through an open or partially-filled duct is characterized by the presence of an air-water interface interacting with a solid wall, forming a mixed-boundary corner. A novel feature of the mixed-boundary corner for turbulent flow is the interaction of wall turbulence with the air-water interface. In the current study, the RANS-VOF equations (for fully developed flow) are solved in a rectangular duct, using periodic inlet/outlet boundary conditions. The flow is completely specified by the (common) driving pressure gradient down the duct and by the fill factor (relative height of the heavier phase to the total height of the duct). Varying the pressure gradient and fill factor results in different flow combinations, namely, laminar air/laminar water, turbulent air/laminar water, turbulent air/turbulent water, laminar air/turbulent water. Since RANS-VOF simulations are computationally less expensive compared to LES and DNS, we systematically investigated a range of flow combinations. The Reynolds stresses are tracked near the mixed-boundary corner for the different flow combinations. The structure of the secondary vortices near the mixed-boundary corner differs from that in the corner formed by the solid vertical and horizontal duct walls.

Keywords: Mixed-boundary corner, density-stratified flow, VOF, two-phase flow, turbulent flow, RANS-RSM modeling

1. Introduction

Flow through an open or partially-filled duct is an important class of flow. This configuration is characterized by the presence of an air-water interface interacting with a solid wall, forming a mixed-boundary corner. Examples of open duct flow, or flow configurations with a mixed-boundary corner, include flow through networks of pipelines transporting crude oil and natural gas, flow in rivers, and flow around ships and other marine structures. An important feature of the mixed-boundary corner is the interaction between wall turbulence and the air-water interface. At a wall boundary, all velocity components vanish, resulting in a region of high shear. By contrast, an air-water interface cannot act as a source of mean shear. The mixed-boundary corner conflates the different behaviors of turbulence at these fundamentally different boundaries, and the resulting complexities affect the transport of mass and momentum [1-4]. Aside from the work of Lee *et al.* [5] previous numerical studies have treated the air-water interface as a non-deforming free-slip boundary. Such a treatment, while retaining the coupling of the two fluids via their mean flow (continuity of velocity and shear stress at the interface), neglects any coupling via the turbulent Reynolds stresses. In such a treatment, the free surface artificially supports a boundary layer, and turbulence is not allowed to communicate across the fluid phases. Lee *et al.*, [5] performed DNS simulations of open-channel flows in the presence of an air-water interface to examine the effects of interface deformation on turbulence structures. In the present study, we focus on the flow features near the mixed-boundary corner.

2. Mathematical Formulation

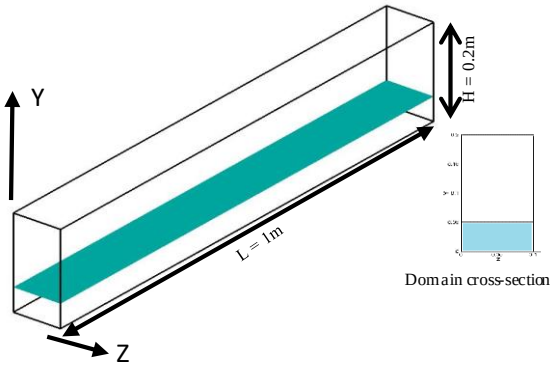

Figure 1. Computational domain

The solution domain (fig. 1) is a partially filled rectangular duct, bounded by no-slip walls, with periodic inlet and outlet boundaries. The total length of the domain is L=1m, and height H=0.2m. The level of water in the domain is specified by h. The fill factor, f = h/H, describes how full the domain is with the heavier fluid.

2.1 Computational details

We perform RANS-VOF simulations of density-stratified, fully developed air-water flow in a 3D rectangular duct, using the finite volume approach (Ansys Fluent 15.0). The discretized form of the governing equations are solved on a structured grid consisting of hexahedral elements. To capture the boundary layers and the interface, the grid is refined along the walls and the interface. Table 1 details the cross-plane grid distribution. The axial direction uses 100 node points. Grid convergence for our 2D simulations was discussed in [6].

Table 1. Cross-plane computational grid details (last three columns denote minimum cell sizes)

f	N_{y_w}	N_{y_a}	N_z	Δy_{wall}	Δy_{fs}	Δz
0.25	30	60	60	$7e^{-4}$	$7e^{-5}$	$7e^{-4}$
0.5	60	60	60	$7e^{-4}$	$7e^{-5}$	$7e^{-4}$
0.75	120	30	60	$7e^{-4}$	$7e^{-5}$	$7e^{-4}$

The discretized equations, along with the initial and boundary conditions, were solved using the segregated solution method to obtain the numerical results. To obtain a good initialization, we adopted a two-step approach. Using previously simulated 2D cases [6], the mass flow rates of the phases crossing the 3D geometry are estimated. These mass flow rates are used as the inlet boundary condition, and hydrostatic pressure is imposed at the outlet. A time-dependent calculation ($\Delta t = 0.01s$) is performed for 120s. The velocity and volume fraction profiles at x/L = 0.5, t = 120s, are used as the inlet condition for a subsequent run. Again, a time-dependent calculation ($\Delta t = 0.01s$) is performed for 100s. The t = 100s solution is used as the initial guess for the time independent calculation with inlet and outlet periodic boundaries. The pressure gradient value required as input for this run is estimated from the solution of the second step. The mass and momentum conservation equations were solved iteratively, and a pressure-correction equation was used to ensure conservation of mass and momentum. The Reynolds stress model (RSM) was used to treat turbulence phenomena in both phases.

2.2 Interface capturing: Volume of fluid (VOF) method

The volume of fluid (VOF) method, which is a surface-capturing technique applied to a fixed Eulerian grid, is used for interface modeling. This model is based on the concept of a phasic volume fraction (denoted here by α, the volume fraction of water in a cell). A value $0 < \alpha < 1$ within a discrete mesh cell represents a segment of interfacial region of two fluids:

- $\alpha = 0$: the cell is empty of water
- $\alpha = 1$: the cell is full of water
- $0 < \alpha < 1$: the cell contains the air-water interface

To compute the time evolution of the interface, we need to move the volume fractions through a grid in a way such that the step function nature of the water volume is maintained.

The kinematic equation for the water volume fraction is a continuity equation:

$$\left[\frac{\partial}{\partial t}(\alpha) + \nabla.(\alpha\vec{v})\right] = 0 \qquad (1)$$

which is solved for the heavier fluid (the secondary fluid). The volume fraction of the lighter fluid (primary fluid) is given by $1 - \alpha$.

The properties appearing in the transport equations namely density and viscosity, are determined by a volume fraction average of all fluids in the cell, *e.g.*, $\rho = \rho_w\alpha + \rho_a(1-\alpha)$. These properties are then used to solve a single momentum equation through the domain, and the computed velocity field is shared among the fluids. The VOF equation is solved using the implicit scheme.

2.3 Governing equations

The governing equations describing the incompressible viscous flow of two immiscible fluids are

The mass conservation equation:

$$\nabla.(\vec{v}) = 0 \quad (2)$$

The RANS momentum conservation equation:

$$U_j \frac{\partial U_i}{\partial x_j} + \frac{1}{\rho}\frac{\partial p}{\partial x} = \frac{1}{\rho}\frac{\partial}{\partial x_j}(\bar{\tau}_{ij} + \lambda_{ij}) \quad (3)$$

here $\bar{\tau}_{ij}$ is the fluid stress tensor, λ_{ij} is the Reynolds stress tensor given by

$$\bar{\tau}_{ij} = -\rho\bar{u}_i\bar{u}_j \quad (4)$$

$$\bar{\lambda}_{ij} = -\rho\overline{u_i'u_j'} \quad (5)$$

The momentum equation is dependent on the volume fractions of all the phases through the properties ρ and μ.

2.4 Turbulence model

The Reynolds stress model (RSM) is used to study the turbulence phenomena. The RSM closes the RANS equations by solving a transport equation for the Reynolds stresses ($\rho\overline{u_i'u_j'}$) appearing in the momentum equations, together with an equation for the dissipation rate.

The flow is driven by a common pressure gradient, which is the input for the numerical simulation. The pressure gradient is estimated as described earlier. We have conducted several simulations at various fill factors and pressure gradients; these are indicated (fig. 2) by the Re of each phase.

3. Results and discussion

Figure 2 depicts the Reynolds number phase diagram, representing the computed Re of the two phases. The Re is calculated based on the average velocity and the hydraulic diameter for each phase. Laminar and turbulent phases are demarcated by dashed lines at Re = 2000. The points represent the computed Re of the 3D simulations at f = ¼, ½, ¾, and their location on graph is representative of the flow combination, namely, turbulent air/laminar water, turbulent air/turbulent water, and, laminar air/turbulent water. Table 2 details the computed Re for the circled points, results for which will be discussed in the remainder of the paper.

Table 2. Computed Reynolds numbers for the two phases

f	dp/dx (Pa)	u_{avg_w} (m/s)	u_{avg_a} (m/s)	Re_a	Re_w
0.25	-0.055	0.014	0.38	3682	1434
0.5	-0.28	0.031	0.44	3788	4070
0.75	-0.14	0.030	0.17	1102	4482

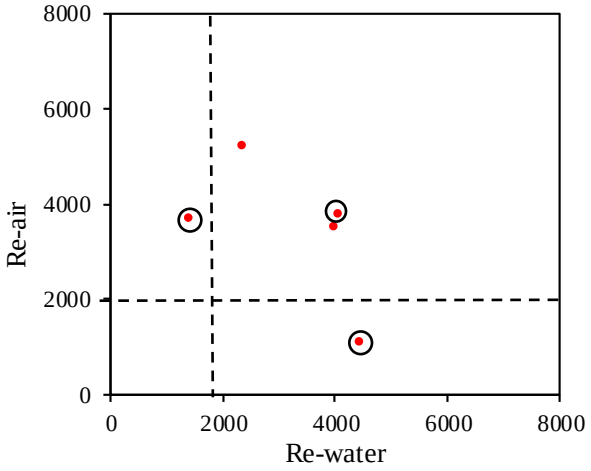

Figure 2. Graphical representation of computed phasic mass flow rates (in terms of Re) at f = ¼, ½, ¾

3.1 Axial velocity

Figure 3 and 4 depict the axial velocity contours and centerline profiles for the three flow scenarios of table 2. When either of the phases is turbulent, the maximum velocity in the heavier phase occurs approximately 5% below the free surface. There is thus a 'velocity dip' at the free surface. Also the maximum velocity of the lighter phase occurs closer to the top wall than to the free surface.

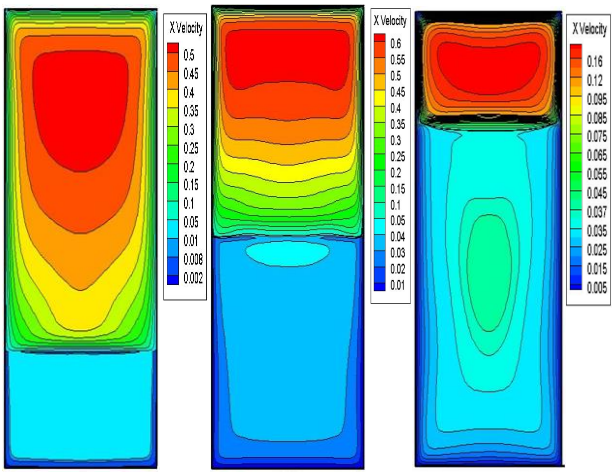

(a) (b) (c)

Figure 3. Axial velocity contours (a) turbulent air/laminar water (b) turbulent air/turbulent water (c) laminar air/turbulent water

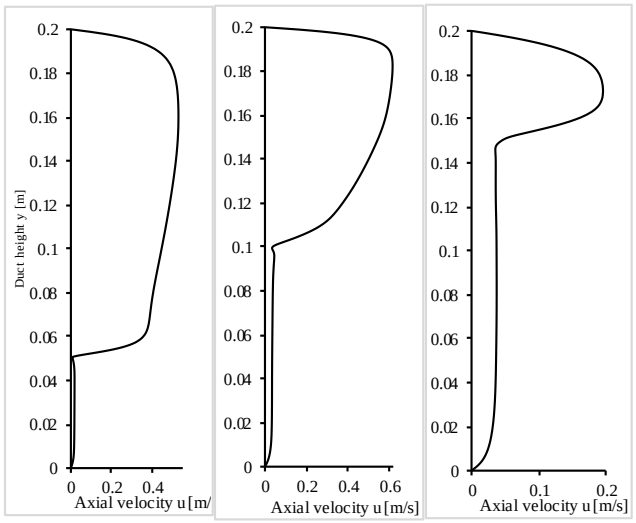

Figure 4. Centerline axial velocity profiles (a) turbulent air/laminar water (b) turbulent air/turbulent water (c) laminar air/turbulent water

3.2 Vorticity Structure

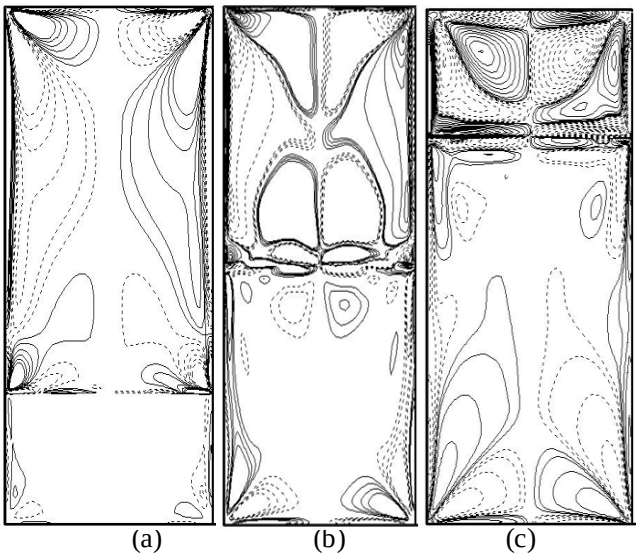

Figure 5. Vorticity contour ωx (a) turbulent air/laminar water (b) turbulent air/turbulent water (c) laminar air/turbulent water

Secondary flow near corners is characteristic of turbulent duct flow. However, the structure of secondary flow near a mixed-boundary corner is very different from that near a wall-wall boundary corner. A wall-wall corner is characterized by a pair of counter-rotating vortices, anti-symmetric about the diagonal. On the other hand, the mixed-boundary corner is characterized by a more complicated vorticity structure which differs between the air and water domains.

In the water domain, irrespective of the Reynolds number, we identify a pair of counter-rotating, narrow vortices which are aligned with the side wall. When turbulent water interacts with either turbulent or laminar air, the narrow vortex pair is accompanied by a larger counter-rotating vortex adjacent to it (fig. 5b, 5c). This larger vortex is missing in the case of turbulent air interacting with laminar water (fig. 5a). Due to leakage at the free surface, even the laminar phase exhibits weak secondary motions as seen in both air and water (fig. 5a and 5c).

In the air phase near the mixed-boundary corner, the structure of the vortex is very different. When turbulent air interacts with laminar water (fig. 5a), the counter-rotating vortices are no longer aligned about the axis of symmetry through the mixed-boundary corner. The vortex structure is somewhat similar to a wall-wall corner, suggesting that the laminar water presents more resistance to the air above, thus acting like a wall. In the case of turbulent air interacting with turbulent water (fig. 5b), the vortex structure in the air domain is quite distorted.

Figure 6 exhibits the ω_y contours for the three flow combinations. In single phase duct flow, the ω_y contours are stacked along the vertical wall going from one corner to the other. On the other hand, a partially filled duct encounters a mixed-boundary corner inside the domain.

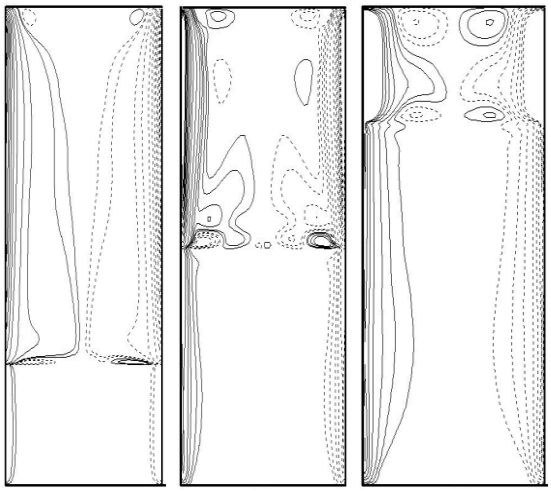

Figure 6. Vorticity contours ω_y (a) turbulent air/laminar water (b) turbulent air/turbulent water (c) laminar air/turbulent water

As a result, in addition to the vertical ω_y contours, horizontal ω_y contours appear at the interface (fig. 6).

Similarly, the ω_z contours in a single phase closed duct are stacked along the width of the duct, extending from one corner to the other. In the case of the partially filled duct, we encounter additional ω_z vortices near the interface (fig. 7).

In the case of turbulent air/laminar water as well as laminar air/turbulent water (fig. 7a and 7c) each phase independently exhibits ω_z contours similar to single phase duct flow. However, in the case of turbulent air/ turbulent water (fig. 7b), a pair of counter-rotating vortices appears in the water domain near the interface.

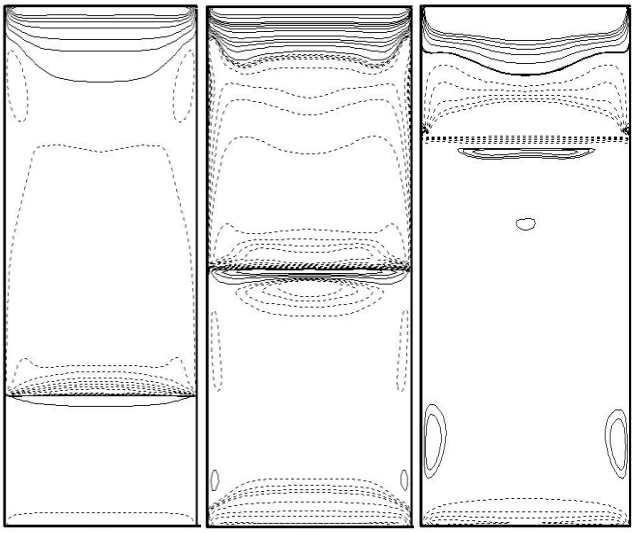

(a) (b) (c)

Figure 7. Vorticity contours ω_z (a) turbulent air-laminar water (b) turbulent air-turbulent water (c) laminar air-turbulent water

The vortex structure near the mixed boundary corner significantly impacts the wall shear stress, $\tau_{zx} = \mu(\frac{\partial u}{\partial z} - \frac{\partial w}{\partial x})$, on the side walls (fig. 8) note, $\frac{\partial w}{\partial x} = 0$ (fully-developed flow). The wall shear stress component τ_{zx} vanishes monotonically at the top and bottom of the duct. It also vanishes at the interface monotonically from the air side, but rises before vanishing at the water side. This increase is attributed to the mixed-boundary vorticity structures.

3.3 Reynolds stresses

Figure 9 (a) - (c) display the diagonal Reynolds stress <u'u'> through the two phases: a) turbulent air/laminar water (f = 0.25); b) turbulent air/turbulent water (f = 0.5); c) laminar air/turbulent water (f = 0.75).

We first discuss the case of turbulent air/laminar water (fig. 9a). The solid wall at the top of the duct acts as a strong source of turbulent fluctuations (the sharp peak on the right). In our RANS VOF simulation, the air-water interface generates turbulent fluctuations in the air, reflecting the fact that the less-mobile water phase acts similarly to a solid wall in generating shear at the interface on the moving air phase. Unlike the moving lid model (where there are no turbulent fluctuations in the laminar water subphase), turbulence fluctuations penetrate into the laminar water subphase and decay with increasing depth.

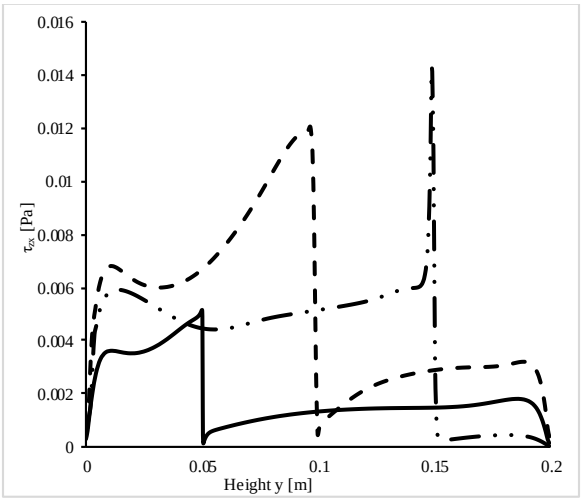

Figure 8. Wall shear stress distribution a)—— f = 0.25, b) - - - - f = 0.5, c) —··—· f = 0.75

The behavior <u'u'> for the case of turbulent air/turbulent water (fig. 9b) is very similar. Again, there is a sharp peak in turbulent fluctuations at the top solid wall, and the air-water interface is a more efficient source of axial fluctuations. The turbulent water phase is expected to display <u'u'> fluctuations; however, the free surface does not act as a solid wall source of such fluctuations, but rather the turbulent fluctuations leak across the interface. The bottom solid surface predictably acts as a weak source of such fluctuations (peak very small on this scale).

The behavior of the axial turbulent fluctuations is counter-intuitive for the case of laminar air/turbulent water (fig. 9c). The bottom solid wall predictably acts as a weak source of axial fluctuations, but, again, this is small on the scale of fig. 9c. Surprisingly, the nominally laminar air exhibits axial turbulent fluctuations, generated both at the free surface and at the solid wall. The ability of the top solid surface to generate a boundary layer with concomitant axial fluctuations is the result of the spatial extent of turbulent fluctuations leaking through into the nominally laminar air-phase.

Figure 9 (d) - (f) display the diagonal vertical Reynolds stress <v'v'> through the two phases: d) turbulent air/laminar water (f = 0.25); e) turbulent air/turbulent water (f = 0.5); f) laminar air/turbulent water (f = 0.75). For the turbulent air cases (fig. 9d, 9e), the magnitude of <v'v'> is about half that of the axial stress <u'u'>; for the laminar air

case (fig. 9f), the magnitude is about one quarter that of the axial stress. The vertical fluctuations necessarily vanish at both top and bottom solid surfaces. The vertical fluctuations are maximal just above the free surface for all cases, and, in all cases, there is significant penetration into the water phase. Again, the vertical fluctuations in the water phase are amplified near the free surface for the laminar air/turbulent water case (fig. 9f). Both features are suppressed in the moving lid approximation.

Figure 9 (g) – (i), display the diagonal cross-plane Re stress <w'w'> through the two phases: (g) turbulent air/laminar water (f = 0.25); h) turbulent air/turbulent water (f = 0.5); i) laminar air/turbulent water (f = 0.75). In magnitude, <w'w'> is comparable to <v'v'>. The horizontal fluctuations necessarily vanish at both top and bottom surfaces. The horizontal fluctuations are maximal just above the free surface in all cases, and, in all cases, there is significant penetration in to the water subphase. For the turbulent air/laminar water (fig. 9g) the water subphase again acts similarly to a solid wall; there are thus two peaks. For the laminar air-turbulent water (fig. 9i), the horizontal fluctuations generated at the bottom surface in the turbulent water phase, are amplified into the free laminar air phase.

Figure 10 (a) – (c) display the off-diagonal Reynolds shear stress <u'v'> through the two phases: a) turbulent air/laminar water (f = 0.25); b) turbulent air/turbulent water (f = 0.5); c) air/turbulent water (f = 0.75). The structure of the off-diagonal stress is qualitatively similar for all three cases. Note the strong peak in the laminar air/turbulent water (fig. 10c), which would vanish in the moving lid model. Figure 10 (d) – (f), display the off-diagonal Re shear stress <u'w'>. The structure is qualitatively similar to <u'v'>. Again, note the strong fluctuations in the laminar air/turbulent water (fig. 10f), which would vanish in the moving lid model. Figure 10 (g) – (i), display the off-diagonal Re stresses <v'w'>. These are an order of magnitude smaller than <u'v'>, <u'w'>. Again, note the strong fluctuations in the laminar air/turbulent water (fig. 10i), which would vanish in the moving lid model.

4. Conclusions

RANS-VOF simulations have been performed of turbulent density-stratified, fully-developed air-water flow in a 3D duct. Varying the pressure gradient (that drives the flow) and the fill factor enables simulations to be performed in all regimes, namely where each of the phases is either laminar or turbulent. The vortex structure near the mixed-boundary corner has been studied in detail, and is found to differ from that seen near a wall boundary corner. The complex vortex structure near the mixed-boundary corner is responsible for the steep increase in the wall shear stress near the interface. The mixed-boundary corner conflates two fundamentally different boundaries and thus different turbulence behavior. The RANS-VOF formulation permits an examination of the rich fluctuation behavior at the interface; such fluctuations are suppressed in the usual moving-lid treatment of the free-surface.

Acknowledgment

This work has been supported in part by NIOSH. This material is declared a work of the U.S. Government and is not subject to copyright protection in the United States. Approved for public release; distribution is unlimited.

Disclaimer

The findings and conclusions in this report are those of the authors and do not necessarily represent the views of the National Institute for Occupational Safety and Health. Mention of product or company name does not constitute endorsement by the Centers for Disease Control and Prevention. None of the authors has a financial relationship with a commercial entity that has an interest in the subject of this manuscript.

References

[1] Broglia, R., Pascarelli, A., and Piomelli, U., 2003, "Large-Eddy Simulations of Ducts with a Free Surface," J. Fluid Mech., **484**(484), pp. 223–253.

[2] Joung, Y., and Choi, S.-U., 2010, "Direct Numerical Simulation of Low Reynolds Number Flows in an Open-Channel with Sidewalls," Int. J. Numer. Methods Fluids, **62**(8), pp. 854–874.

[3] Grega, L. M., Hsu, T. Y., and Wei, T., 2002, "Vorticity Transport in a Corner Formed by a Solid Wall and a Free Surface," J. Fluid Mech., **465**, pp. 331–352.

[4] Shi, J., Thomas, T. G., and Williams, J. J. R., 1999, "Large-Eddy Simulation of Flow in a Rectangular Open Channel," J. Hydraul. Res., **37**(3), pp. 345–361.

[5] Lee, J., Suh, J., and Sung, H. J., 2011, "Direct Numerical Simulation of Turbulent Open Channel Flow with Froude Number Effect," 7th Int. Symp. Turbul. Shear Flow Phenom.

[6] Jana, C., Ghia, U., and Turkevich, L.A,. J., 2011, "RANS-VOF Simulations of Density-Stratified Air-Water Flow in a 2D Channel," Proce of the ASME 2020 Fluids Eng. Div. Summer Meeting, Vol 1, FEDSM 2020-20388.

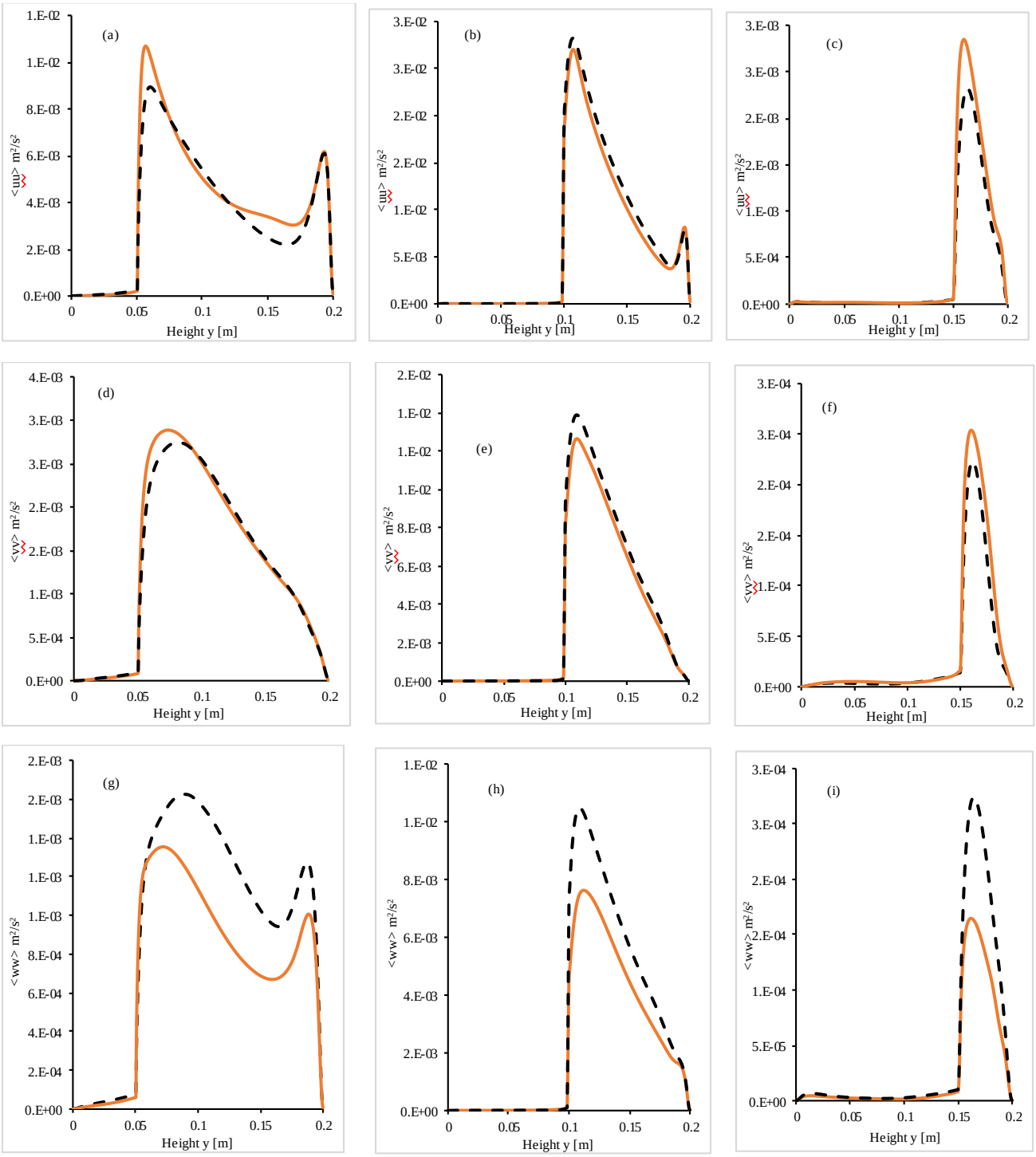

Figure 9. Diagonal Reynolds stress profiles at f = 0.25, 0.5, 0.75: (a) – (c) <u'u'>; (d) – (f) <v'v'>; (g) – (i) <w'w'>; — z = 0.02, – – z = 0.05

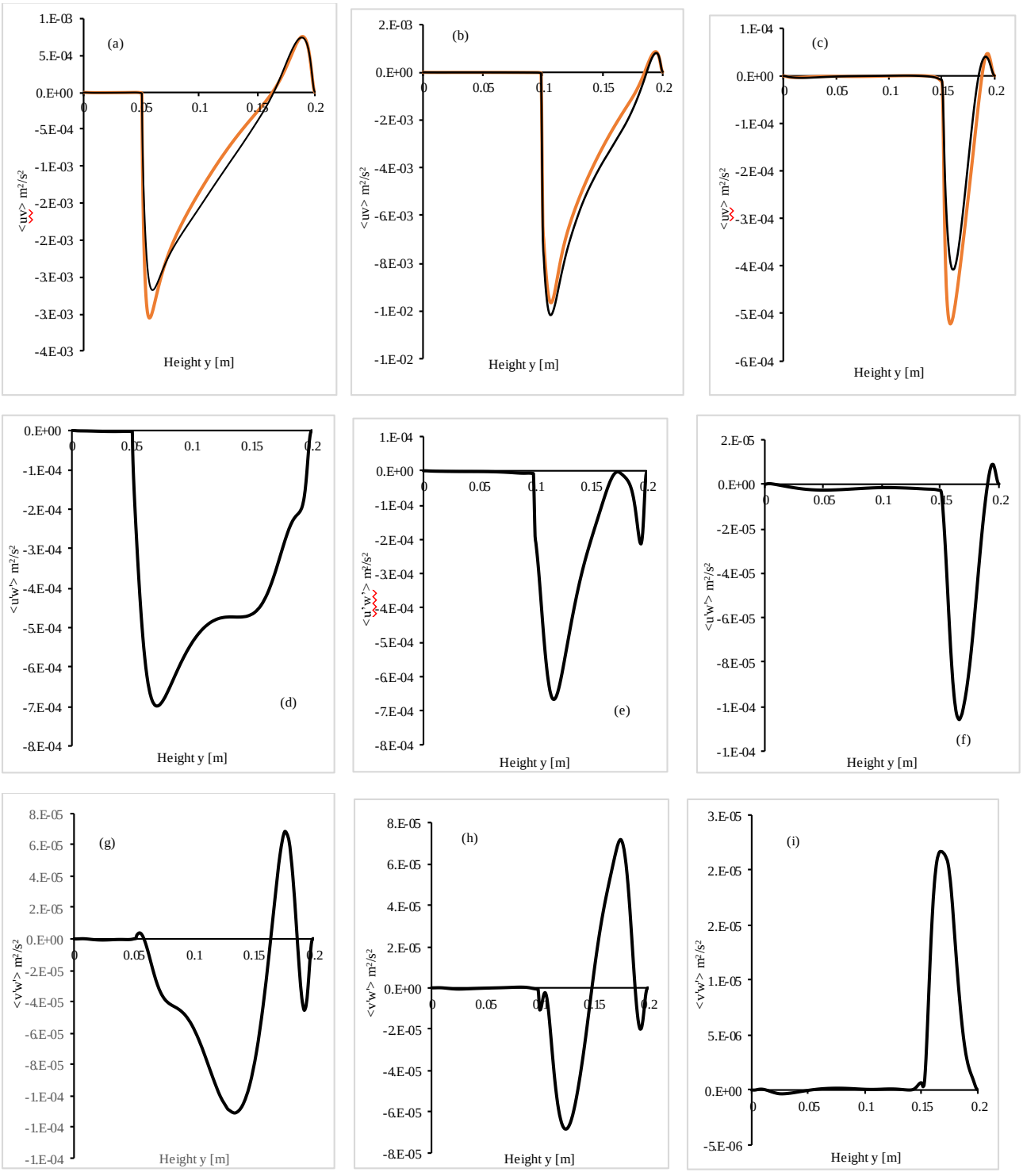

Figure 10. Off-Diagonal Reynolds stress profiles at f = 0.25, 0.5, 0.75: (a) – (c) <u'v'>; (d) – (f) <u'w'>; (g) – (i) <v'w'>
z = 0.02, z = 0.05